Hindawi
Mathematical Problems in Engineering
Volume 2021, Article ID 5533920, 19 pages
https://doi.org/10.1155/2021/5533920

Research Article

Free Vibration Investigations of Rotating FG Beams Resting on Elastic Foundation with Initial Geometrical Imperfection in Thermal Environments

Dang Nguyen Van

University of Transport Technology, 54 Trieu Khuc, Thanh Xuan, Hanoi, Vietnam

Correspondence should be addressed to Dang Nguyen Van; dangnv@utt.edu.vn

Received 3 February 2021; Revised 5 April 2021; Accepted 28 April 2021; Published 11 May 2021

Academic Editor: Z. Du

In practical operations of mechanical structures, it is not difficult to meet some large components such as helicopter rotors, gas turbine blades of marine engines, and rotating railway bridges, where these elements can be seen as beam models rotating around one fixed axis. Therefore, mechanical explorations of these structures with and without the effect of temperature will guide the design, manufacture, and use of them in practice. This is the first paper that uses the shear deformation theory-type hyperbolic sine functions and the finite element method to analyze the free vibration response of rotating FGM beams with initial geometrical imperfections resting on elastic foundations considering the effect of temperature. The material properties are assumed to be varied in the thickness direction of the beam based on the power law function and temperature changes The proposed theory and mathematical model are verified by comparing the results with other exact solutions. The numerical investigations have taken into account some geometrical and material parameters to evaluate the effects on the vibration behavior of the structure such as the rotational speed, temperature, as well as initial geometrical imperfections. The drawn comments have numerous scientific and practical implications for rotating beam structures.

1. Introduction

Functionally graded materials (FGM) are made of two or more different materials, where the common type is the combination of ceramic and metal with the changing law of material properties in one direction. Due to the ceramic component in the composition, the structures made of FG materials have good heat resistance, and they are usually designed for use in high-temperature environments. Therefore, the research on the mechanical behavior of structures made of these materials, including FGM beams, has interested scientists worldwide [1–5]. Besides, in engineering practice, some parts of turbines, aircraft propellers, and so on can be seen as beam structures with rotational movements. The following publications related to these structures can be counted. Gunjal and Dixit [6] studied the minimum of the vibrations of rotating beams through the shape optimization of these beams, in which the finite element method was used to model the rotating beam and sequential quadratic programming was used for the optimization process. Pradhan and Murmu [7] used Eringen's nonlocal elasticity theory and a single nonlocal beam model to investigate the mechanical behavior of a rotating nanobeam, where the differential quadrature method was adopted in this work. Li et al. [8] examined the free vibration response of a rotating functionally graded material (FGM) beam using a dynamic model; the results took the effects of the bending and stretching phenomena into account. Amir et al. [9] explored the lead-lag vibration problem of rotating microbeams based on Euler–Bernoulli and Timoshenko beam theories and the finite element method. Jung-Woo and Jung-Youn [10] studied the effects of cracks on the natural frequencies of a rotating Bernoulli–Euler beam by employing a new numerical approach, where these effects could be computed simply using the transfer matrix method. Das [11] employed the Ritz method to calculate the in-plane

and out-of-plane mechanical behavior of the rotating FGM beam, which was based on the Timoshenko beam theory and the Coriolis acceleration. Xu et al. [12] investigated the dynamic model and vibration suppression of a rotating cantilever beam under magnetic excitations based on the Hamilton principle and Galerkin method. The free vibration response analysis of the rotating rod based on Eringen's nonlocal elasticity was carried out by Alireza and Cai [13]. Liang et al. [14] studied the vibration control of a rotating piezoelectric FGM beam in thermal environments by using the high-order coupling modeling theory. Dejin et al. [15] introduced a combination of the Timoshenko beam and remodified couple stress theories to capture the free vibration response of rotating microbeams, in which the beams were made from multilayered composite components with geometric imperfections. Euler–Bernoulli's beam, Eringen's nonlocal elasticity theories, and Galerkin method were employed by Atanasov and Stojanovic [16] to investigate the free vibration of rotating nanobeams, in which a wide range of parameter studies was carried out, especially the speed of rotation around one fixed axis.

In addition, for structures made of pore-defect materials, structures resting on elastic foundations and structures taking into account the effect of temperature have been also investigated by scientists worldwide. Jalaei and Civalek [17] used Navier's solution and Bolotin's approach to study the dynamic instability of viscoelastic porous functionally graded nanobeam embedded on visco-Pasternak medium. Demir and Civalek [18] investigated the bending of nano/microbeams under the concentrated and distributed loads using Euler–Bernoulli beam theory via the enhanced Eringen differential model. Akgoz and Civalek [19] introduced the exact solution for the static bending and buckling problems of simply supported microbeams embedded in an elastic medium. The exact solution was also presented by Hanten et al. [20] to analyze the free vibration analysis of beams made of fibre-metal laminated beams. The research on the mechanical behavior of plate and beam structures resting on different elastic foundations has been studied by scientists, typically in works [21–30]. In works [27, 29, 31–35], the authors explored the mechanical response of beams and plates taking into account the effect of temperature with numerous different theories.

Based on the review above, it can be seen that there are not any publications on free vibration responses of rotating FGM beams resting on elastic foundations in thermal environments, in which geometrical imperfections are taken into account. Hence, this paper is about to explore the free vibration behavior of these structures by using the combination of the finite element method and the new type of hyperbolic sine functions of shear deformation theory. The proposed theory is simple and easy to establish the stress and strain relations, which does not need to add any shear correction factors, while the mechanical phenomena are still desired exactly.

The rest of this paper is structured as follows. Finite element formulations of the rotating FGM beam in a thermal environment are presented in Section 2, where geometrical imperfections and temperature effects are considered. Section 3 conducts verification examples to evaluate the accuracy of the proposed theory and mechanical models. Numerical data and discussions are located in Section 4. Section 5 concludes some remarkable points of this work.

2. Finite Element Model of the Rotating FGM Beam in a Thermal Environment

Consider a functionally graded material (FGM) beam rotating around one fixed axis with the speed χ. One side of the beam is at distance r from the fixed axis Δ. The beam is resting on a two-parameter elastic foundation k_w and k_s, as shown in Figure 1. The beam has dimensions such as the length L, width b, and thickness h, and an initial geometric imperfection in the z-direction is $w_{\text{im}}(x)$.

The beam structure is made from ceramic (denoted by c) and metal (denoted by m), in which volume proportions (V_c and V_m) are varied according to the thickness direction based on the following power law function [1, 36–39]:

$$V_c = \left(\frac{z}{h} + \frac{1}{2}\right)^n, \qquad V_m = 1 - V_c, \quad \text{with } n \geq 0, \tag{1}$$

where z is the thickness coordinate variable with $-h/2 \leq z \leq h/2$ and n is the volume fraction index and its variation. From equation (1), one can see that, at the top surface of the beam ($z = h/2$), it has $V_c = 1$ and $V_m = 0$, i.e., full ceramic at this surface, and at the bottom surface of the beam is completely metallic, and two ceramic and metal materials change continuously from one surface to the other surface of the beam in the thickness direction.

Young's modulus E, density ρ, Poisson's ratio ν, and coefficient of the thermal expansion α are functions of the power law distribution as [1]:

$$\begin{aligned} E(z) &= E_m + (E_c - E_m)\left(\frac{1}{2} + \frac{z}{h}\right)^n, \\ \rho(z) &= \rho_m + (\rho_c - \rho_m)\left(\frac{1}{2} + \frac{z}{h}\right)^n, \\ \nu(z) &= \nu_m + (\nu_c - \nu_m)\left(\frac{1}{2} + \frac{z}{h}\right)^n, \\ \alpha(z) &= \alpha_m + (\alpha_c - \alpha_m)\left(\frac{1}{2} + \frac{z}{h}\right)^n. \end{aligned} \tag{2}$$

The beam is assumed to be placed in a thermal environment; as a result, the material properties are varied by the temperature as follows [40]:

$$P = P_0\left(P_{-1}T^{-1} + 1 + P_1 T + P_2 T^2 + P_3 T^3\right), \tag{3}$$

where $T = T_0 + \Delta T$, ΔT is the temperature increment, $T_0 = 300K$ is the room temperature (this temperature also does not affect the stress of the material), and P_0, P_{-1}, P_1, P_2, and P_3 are constants depending on different materials.

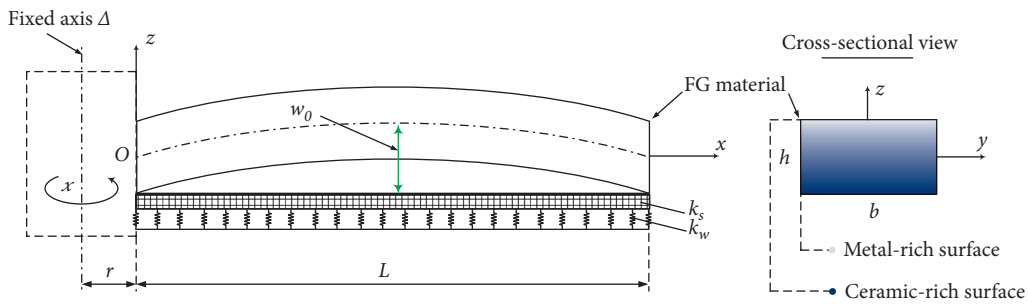

Figure 1: A rotating FGM beam with the initial geometric imperfection.

To represent properly the mechanical behaviors of FGM beams, this work uses a new shear deformation theory-type hyperbolic sine functions; thus, the displacements u and w in the x- and z-directions at any point with the coordinate (x, z) are expressed as follows [41, 42]:

$$\begin{cases} u(x,z) = u_0(x,y) - z\dfrac{\partial w_b}{\partial x} - f(z)\dfrac{\partial w_s}{\partial x}, \\ w(x,z) = w_b + w_s + w_{\text{im}}(x), \end{cases} \tag{4}$$

in which $f(z) = z - h\sinh(z/h) + z\cosh(1/2)$.

The longitudinal and shear strains of the beam are defined as follows:

$$\begin{aligned} \varepsilon_{xx} &= \frac{\partial u}{\partial x} = \frac{\partial u_0}{\partial x} - z\frac{\partial^2 w_b}{\partial x^2} - f(z)\frac{\partial^2 w_s}{\partial x^2} + \frac{\mathrm{d}w_{\text{im}}}{\mathrm{d}x}\frac{\partial(w_b + w_s)}{\partial x} - \varepsilon_T, \\ &= \frac{\partial u_0}{\partial x} + z\left(-\frac{\partial^2 w_b}{\partial x^2}\right) + f(z)\left(-\frac{\partial^2 w_s}{\partial x^2}\right) + \frac{\mathrm{d}w_{\text{im}}}{\mathrm{d}x}\frac{\partial(w_b + w_s)}{\partial x} - \varepsilon_T, \\ &= \varepsilon_{0x} + z\varepsilon_{bx} + f(z)\varepsilon_{sx} + \varepsilon_{\text{im}} - \varepsilon_T, \\ \gamma_{xz} &= \frac{\partial f(z)}{\partial z}\frac{\partial w_s}{\partial x} = \frac{\partial f(z)}{\partial z}\gamma_{sxz}, \end{aligned} \tag{5a}$$

in which the strain components have the following expressions:

$$\begin{aligned} \varepsilon_{0x} &= \frac{\partial u_0}{\partial x}, \\ \varepsilon_{bx} &= \left(-\frac{\partial^2 w_b}{\partial x^2}\right), \\ \varepsilon_{sx} &= \left(-\frac{\partial^2 w_s}{\partial x^2}\right), \\ \varepsilon_{\text{im}} &= \frac{\mathrm{d}w_0}{\mathrm{d}x}\frac{\partial(w_b + w_s)}{\partial x}, \\ \gamma_{sxz} &= \frac{\partial w_s}{\partial x}. \end{aligned} \tag{5b}$$

The normal stresses relating to the mechanical strain σ_{xx}, the thermal strain σ_T, and the shear stress τ_{xz} have the following expressions:

$$\begin{cases} \sigma_{xx} = E(z)\varepsilon_{xx}; \\ \sigma_T = E(z)\varepsilon_T, \\ \tau_{xz} = \dfrac{E(z)}{2(1+\nu(z))}\gamma_{xz}, \end{cases} \tag{6}$$

where the strain relating to the temperature is $\varepsilon_T = \alpha(z)(T - T_0)$.

The energy of the FGM beam is calculated as

$$U^E = \frac{1}{2}\int_V \left(\sigma_{xx}^T \varepsilon_{xx} + \tau_{xz}^T \gamma_{xz}\right) \mathrm{d}V = \frac{1}{2}\int_V \left(\left\{ \varepsilon_{0x} \;\; z\varepsilon_{bx} \;\; f(z)\varepsilon_{sx} \;\; \varepsilon_{\mathrm{im}} \right\}^T E \begin{Bmatrix} \varepsilon_{0x} \\ z\varepsilon_{bx} \\ f(z)\varepsilon_{sx} \\ \varepsilon_{im} \end{Bmatrix} \right) \mathrm{d}V$$

$$+ \frac{1}{2}\int_V \left(\left\{ \frac{\partial f(z)}{\partial z} \gamma_{sxz} \right\}^T \frac{E(z)}{2(1+\nu(z))} \left\{ \frac{\partial f(z)_{sxz}}{\partial z \;\; \gamma} \right\} \right) \mathrm{d}V,$$

$$\frac{1}{2}\int_V \begin{pmatrix} \varepsilon_{0x}^T E(z)\varepsilon_{0x} + \varepsilon_{0x}^T z E(z)\varepsilon_{bx} + \varepsilon_{0x}^T f(z) E(z)\varepsilon_{sx} + \varepsilon_{0x}^T E(z)\varepsilon_{\mathrm{im}} \\ \varepsilon_{bx}^T E(z) z\varepsilon_{0x} + \varepsilon_{bx}^T E(z) z^2 \varepsilon_{bx} + \varepsilon_{bx}^T E(z) z f(z)\varepsilon_{sx} + \varepsilon_{bx}^T E(z) z\varepsilon_{\mathrm{im}} \\ \varepsilon_{sx}^T E(z) f(z)\varepsilon_{0x} + \varepsilon_{sx}^T E(z) z f(z)\varepsilon_{bx} + \varepsilon_{sx}^T E(z) f^2(z)\varepsilon_{sx} + \varepsilon_{sx}^T E(z) f(z)\varepsilon_{\mathrm{im}} \\ \varepsilon_{\mathrm{im}}^T E(z)\varepsilon_{0x} + \varepsilon_{\mathrm{im}}^T E(z) z\varepsilon_{bx} + \varepsilon_{\mathrm{im}}^T E(z) f(z)\varepsilon_{sx} + \varepsilon_{\mathrm{im}}^T E(z)\varepsilon_{\mathrm{im}} \end{pmatrix} \mathrm{d}V$$

$$+ \frac{1}{2}\int_V \left(\left(\frac{\partial f(z)}{\partial z} \right)^2 \frac{E(z)}{2(1+\nu(z))} \gamma_{sxz}^T \gamma_{sxz} \right) \mathrm{d}V. \tag{7}$$

The energy of the elastic foundation is defined as

$$U^F = \frac{1}{2} b \int_L \left(k_w (w_b + w_s)^2 + k_s \left(\frac{\partial((w_b + w_s))}{\partial x} \right)^2 \right) \mathrm{d}x, \tag{8}$$

where k_w and k_s are the two coefficients of the elastic foundation.

The FGM beam rotates around one axis Δ with the rotational speed χ; therefore, the potential energy of this structure generated by the rotational movement is defined as follows [15, 43]:

$$U^R = \frac{1}{2}\int_L \left(F_\chi(x) \left(\frac{\partial(w_b + w_s)}{\partial x} \right)^2 \right) \mathrm{d}x, \tag{9}$$

with the centrifugal force F_χ is calculated as follows [15]:

$$F_\chi = \frac{1}{2}\int_S \left(\rho(z)\chi^2 \left[r(L-x) + \frac{1}{2}\left(L^2 - x^2\right) \right] \right) \mathrm{d}S, \tag{10}$$

in which $\rho(z)$ is the density of the material.

The work done by temperature acting in the longitudinal direction of the FGM beam is defined as follows [43]:

$$U^{Th} = \frac{1}{2}\int_V \left(\sigma_T \left(\frac{\partial(w_b + w_s)}{\partial x} \right)^2 \right) \mathrm{d}V. \tag{11}$$

The kinetic energy of the beam is expressed as follows:

$$D = \frac{1}{2}\int_V \rho(z) \left(\left(\frac{\partial \dot{u}^T}{\partial t} \right) \left(\frac{\partial \dot{u}}{\partial t} \right) + \left(\frac{\partial \dot{w}^T}{\partial t} \right) \left(\frac{\partial \dot{w}}{\partial t} \right) \right) \mathrm{d}V. \tag{12}$$

To determine the equilibrium equation of the FGM beam, this work uses Hamilton's principle:

$$\delta \int_{t_1}^{t_2} \left(D - U^E - U^F - U^{Ro} + U^{Th} \right) \mathrm{d}t = 0. \tag{13}$$

In this paper, a two-node beam element is employed, where each node contains four degrees of freedom:

$$\mathbf{q}_e = \sum_{i=1}^{2} \begin{Bmatrix} u_{0i} \\ w_{bi} \\ w_{si} \\ \left(\frac{\partial w_b}{\partial x} \right)_i \\ \left(\frac{\partial w_s}{\partial x} \right)_i \end{Bmatrix}, \tag{14}$$

where the displacement components at each point within the beam element are approximated through Lagrange and Hermite interpolation functions N_i and H_i:

$$\begin{cases} u_0 = \sum_{i=1}^{2} N_i u_{0i} = \mathbf{N}_u \mathbf{q}_e, \\ w_b = \sum_{i=1}^{2} \left\{ H_i w_{bi} + H_{i+1} \left(\frac{\partial w_b}{\partial x} \right)_i \right\} = \mathbf{H}_b \mathbf{q}_e, \\ w_s = \sum_{i=1}^{2} \left\{ H_i w_{si} + H_{i+1} \left(\frac{\partial w_s}{\partial x} \right)_i \right\} = \mathbf{H}_s \mathbf{q}_e, \\ \frac{\partial w_b}{\partial x} = \sum_{i=1}^{2} \left\{ \frac{\partial H_i}{\partial x} w_{bi} + \frac{\partial H_{i+1}}{\partial x} \left(\frac{\partial w_b}{\partial x} \right)_i \right\} = \mathbf{H}_{bx} \mathbf{q}_e, \\ \frac{\partial w_s}{\partial x} = \sum_{i=1}^{2} \left\{ \frac{\partial H_i}{\partial x} w_{si} + \frac{\partial H_{i+1}}{\partial x} \left(\frac{\partial w_s}{\partial x} \right)_i \right\} = \mathbf{H}_{sx} \mathbf{q}_e, \\ \frac{\partial^2 w_b}{\partial x^2} = \sum_{i=1}^{2} \left\{ \frac{\partial^2 H_i}{\partial x^2} w_{bi} + \frac{\partial^2 H_{i+1}}{\partial x^2} \left(\frac{\partial w_b}{\partial x} \right)_i \right\} = \mathbf{H}_{b2x} \mathbf{q}_e, \\ \frac{\partial^2 w_s}{\partial x^2} = \sum_{i=1}^{2} \left\{ \frac{\partial^2 H_i}{\partial x^2} w_{si} + \frac{\partial^2 H_{i+1}}{\partial x^2} \left(\frac{\partial w_s}{\partial x} \right)_i \right\} = \mathbf{H}_{s2x} \mathbf{q}_e, \end{cases} \tag{15}$$

or, in the matrix form as

$$\mathbf{u} = \begin{Bmatrix} u_0 \\ w_b \\ w_s \\ \left(\frac{\partial w_b}{\partial x} \right) \\ \left(\frac{\partial w_s}{\partial x} \right) \end{Bmatrix} = \begin{bmatrix} \mathbf{N}_u \\ \mathbf{H}_b \\ \mathbf{H}_s \\ \mathbf{H}_{bx} \\ \mathbf{H}_{sx} \end{bmatrix} \mathbf{q}_e = \mathbf{H} \mathbf{q}_e. \tag{16}$$

And, strain components are calculated according to the nodal displacement as follows:

$$\begin{cases} \varepsilon_{0x} = \frac{\partial u_0}{\partial x} = \frac{\partial N_u}{\partial x} \mathbf{q}_e = \mathbf{B}_u \mathbf{q}_e, \\ \varepsilon_{bx} = -\frac{\partial^2 w_b}{\partial x^2} = -\mathbf{H}_{b2x} \mathbf{q}_e = \mathbf{B}_b \mathbf{q}_e, \\ \varepsilon_{sx} = -\frac{\partial^2 w_s}{\partial x^2} = -\mathbf{H}_{s2x} \mathbf{q}_e = \mathbf{B}_s \mathbf{q}_e, \\ \varepsilon_{\mathrm{imp}} = \frac{\partial (w_b + w_s)}{\partial x} \frac{\mathrm{d} w_{\mathrm{im}}}{\mathrm{d} x} = \frac{\mathrm{d} w_{\mathrm{im}}}{\mathrm{d} x} (\mathbf{H}_b + \mathbf{H}_s) \mathbf{q}_e = \mathbf{B}_{\mathrm{im}} \mathbf{q}_e, \end{cases}$$

$$\gamma_{sxz} = \frac{\partial w_s}{\partial x} = \mathbf{H}_{sx} \mathbf{q}_e. \tag{17}$$

One can get the energy expression of the FGM beam element as follows:

$$
\begin{aligned}
U_e^E &= \frac{1}{2}\mathbf{q}_e^T \int_V \begin{pmatrix} \mathbf{B}_u^T E \mathbf{B}_u + \mathbf{B}_u^T z E \mathbf{B}_b + \mathbf{B}_u^T f(z) E \mathbf{B}_s + \mathbf{B}_u^T E \mathbf{B}_{\mathrm{im}} \\ \mathbf{B}_b^T E z \mathbf{B}_u + \mathbf{B}_b^T E z^2 \mathbf{B}_b + \mathbf{B}_b^T E z f(z) \mathbf{B}_s + \mathrm{B}_b^T E z \mathbf{B}_{\mathrm{im}} \\ \mathbf{B}_s^T E f(z) \mathbf{B}_u + \mathbf{B}_s^T E z f(z) \mathbf{B}_b + \mathbf{B}_s^T E f^2(z) \mathbf{B}_s + \mathbf{B}_s^T E f(z) \mathbf{B}_{\mathrm{im}} \\ \mathbf{B}_{\mathrm{im}}^T E \mathbf{B}_u + \mathbf{B}_{\mathrm{imp}}^T E z \mathbf{B}_b + \mathbf{B}_{\mathrm{imp}}^T E f(z) \mathbf{B}_s + \mathbf{B}_{\mathrm{im}}^T E \mathbf{B}_{\mathrm{im}} \end{pmatrix} \mathrm{d}V \mathbf{q}_e \\
&\quad + \frac{1}{2}\mathrm{q}_e^T \int_V \left(\left(\frac{\partial f(z)}{\partial z} \right)^2 \frac{E}{2(1+\nu)} \mathbf{H}_{sx}^T \mathbf{H}_{sx} \right) \mathrm{d}V \mathbf{q}_e, \\
&= \frac{1}{2}\mathbf{q}_e^T \int_V \begin{pmatrix} \mathbf{B}_u^T E \mathbf{B}_u + \mathbf{B}_u^T z E \mathbf{B}_b + \mathbf{B}_u^T f(z) E \mathbf{B}_s + \mathbf{B}_u^T E \mathbf{B}_{\mathrm{im}} \\ \mathbf{B}_b^T E z \mathbf{B}_u + \mathbf{B}_b^T E z^2 \mathbf{B}_b + \mathbf{B}_b^T E z f(z) \mathbf{B}_s + \mathbf{B}_b^T E z \mathbf{B}_{\mathrm{im}} \\ \mathbf{B}_s^T E f(z) \mathbf{B}_u + \mathbf{B}_s^T E z f(z) \mathbf{B}_b + \mathbf{B}_s^T E f^2(z) \mathbf{B}_s + \mathbf{B}_s^T E f(z) \mathbf{B}_{\mathrm{im}} \\ \mathbf{B}_{\mathrm{im}}^T E \mathbf{B}_u + \mathbf{B}_{\mathrm{imp}}^T E z \mathbf{B}_b + \mathrm{B}_{\mathrm{imp}}^T E f(z) \mathbf{B}_s + \mathbf{B}_{\mathrm{im}}^T E \mathbf{B}_{\mathrm{im}} \end{pmatrix} \mathrm{d}V \mathbf{q}_e \\
&\quad + \frac{1}{2}\mathbf{q}_e^T \int_V \left(\left(\frac{\partial f(z)}{\partial z} \right)^2 \frac{E}{2(1+\nu)} \mathbf{H}_{sx}^T \mathbf{H}_{sx} \right) \mathrm{d}V \mathbf{q}_e.
\end{aligned} \tag{18}
$$

Equation (18) can be rewritten in the short form as follows:

$$
U_e^E = \frac{1}{2}\mathbf{q}_e^T \mathbf{K}_e^E \mathbf{q}_e. \tag{19}
$$

The energy of the centrifugal inertia force and the elastic foundation is calculated as follows:

$$
\begin{aligned}
U_e^F &= \frac{1}{2}\mathbf{q}_e^T \left(b \int_L \left(k_w (\mathbf{H}_b + \mathbf{H}_s)^T (\mathbf{H}_b + \mathbf{H}_s) + k_s (\mathbf{H}_{bx} + \mathbf{H}_{sx})^T (\mathbf{H}_{bx} + \mathbf{H}_{sx}) \right) \mathrm{d}x \right) \mathbf{q}_e = \frac{1}{2}\mathbf{q}_e^T \mathbf{K}_e^F \mathbf{q}_e, \\
U_e^R &= \frac{1}{2}\mathbf{q}_e \left(\int_L \left\{ F_\chi(x) (\mathbf{H}_{bx} + \mathbf{H}_{sx})^T (\mathbf{H}_{bx} + \mathbf{H}_{sx}) \right\} \mathrm{d}x \right) \mathbf{q}_e = \frac{1}{2}\mathbf{q}_e^T \mathbf{K}_e^R \mathbf{q}_e.
\end{aligned} \tag{20}
$$

The energy generated by the thermal strain is calculated as follows:

$$
U^{Th} = \frac{1}{2} \int_V \left(\sigma_T (\mathbf{H}_{bx} + \mathbf{H}_{sx})^T (\mathbf{H}_{bx} + \mathbf{H}_{sx}) \right) \mathrm{d}V = \frac{1}{2}\mathbf{q}_e^T \mathbf{K}_e^{Th} \mathbf{q}_e, \tag{21}
$$

where σ_T is given in equation (6).

The kinetic energy of the FGM beam element is determined as follows:

$$
D_e = \frac{1}{2} \int_V \left(\dot{u}^T \rho(z) \dot{u} \right) \mathrm{d}V = \frac{1}{2}\dot{q}_e^T \left(\int_V \left(\mathbf{H}^T \mathbf{H} \right) \mathrm{d}V \right) \dot{q}_e = \frac{1}{2}\dot{q}_e^T (\mathbf{M}_e) \dot{q}_e, \tag{22}
$$

in which $\mathbf{M}_e = \int_V \rho(z) (\mathbf{H}^T \mathbf{H}) \mathrm{d}V$ is the element mass matrix.

By substituting equations (18)–(20) into (13), the equation to get the fundamental frequency as well as vibration mode shape of the rotating FGM beam is obtained as follows:

$$
\left\{ \sum_e \left(\mathbf{K}_e^E + \mathbf{K}_e^F + \mathbf{K}_e^R - \mathbf{K}_e^{Th} \right) - \omega^2 \sum_e \mathbf{M}_e \right\} \sum_e \mathbf{q}_e = 0. \tag{23}
$$

Equation (23) proves that all components related to rotational speed, elastic foundation parameter, initial geometrical imperfection, and temperature are presented in the equation for determining the specific vibration response of the FGM beam, which is completely different from traditional beams, which make the computation more complicated in comparison with previous studies. It should also be noted that, in equation (23), the global stiffness matrix $\mathbf{K} = \sum_e (\mathbf{K}_e^E + \mathbf{K}_e^F + \mathbf{K}_e^R - \mathbf{K}_e^{Th})$, the global mass matrix $\mathbf{M} = \sum_e \mathbf{M}_e$, and the global vector $\mathbf{q} = \sum_e \mathbf{q}_e$ depend on specific boundary conditions. Here is the deletion of rows and columns corresponding to zero degrees of freedom at the boundary nodes, which are described as follows:

(i) Simply supported (represented by S):

$$u_0 = 0,\quad w_b = 0,\quad w_s = 0. \tag{24}$$

(ii) Clamped (represented by C):

$$u_0 = 0,\quad w_b = 0,\quad w_s = 0,\quad \frac{\partial w_b}{\partial x} = 0,\quad \frac{\partial w_s}{\partial x} = 0. \tag{25}$$

(iii) Free (represented by F):

$$u_0 \neq 0,\quad w_b \neq 0,\quad w_s \neq 0,\quad \frac{\partial w_b}{\partial x} \neq 0,\quad \frac{\partial w_s}{\partial x} \neq 0. \tag{26}$$

This work calculates for FGM beams with three boundary conditions.

(i) One side is clamped, and the other side is free: C-F

(ii) Fully simply supported beam: S-S

(iii) Fully clamped beam: C-C

3. Verification Study

This section considers 4 examples to evaluate the accuracy of the proposed theory and mechanical model, where the numerical results of this work are compared with those of other trustful papers.

Example 1. Firstly, this example compares the results of frequencies of the FGM (Al/Al_2O_3) beam resting on a two-parameter elastic foundation with simply supported boundaries at two sides of the beam. Geometrical and material parameters are the length L, thickness h, $L/h = 100$, width b, $E_m = 70$ GPa, $\rho_m = 2702$ kg/m^3, $E_c = 380$ GPa, and$\rho_c = 3960$ kg/m^3. Two non-dimensional frequencies of the elastic foundation are defined as follows:

$$\begin{cases} \overline{K}_w = \dfrac{K_1 L^4}{E_m I}, \\ \overline{K}_s = \dfrac{K_2 L^2}{E_m I \pi^2}, \end{cases} \tag{27a}$$

with

$$I = \frac{bh^3}{12}. \tag{27b}$$

The nondimensional frequency of the beam is defined by the following formula:

$$\widehat{\omega} = \omega_1 \frac{L^2}{h}\sqrt{\frac{\rho_m}{E_m}}. \tag{28}$$

Table 1 presents the results of this work and the analytical method [44], where this work carries out some different mesh sizes. It can be observed that, with the 10-element mesh size, the accuracy is acceptable; therefore, this work will use this mesh for all following sections.

Example 2. Next, this problem carries the comparison of frequencies of the fully simply supported FGM beam with initial geometrical imperfection. The beam has the following parameter: $L = 288.7$ h, $h = 0.02$ m, $b = 0.04$ m, $E = 971$ GPa, and mass density $\rho = 2300$ kg/m^3. The initial imperfection of the beam is $w_{\text{im}}(x) = J_0 \sin(\pi x)$, where J_0 is the amplitude of imperfection. The first nondimensional frequency and the initial imperfection coefficient ς_0 are defined as follows:

$$\omega^{**} = \omega_1 \sqrt{\frac{12\rho L^4}{Eh^2}},\quad \varsigma_0 = \frac{J_0}{L}. \tag{29}$$

The first nondimensional frequencies of the S-S FGM beam with initial geometrical imperfection obtained from this work and the pseudo-arclength continuation technique [45] in the case of increasing gradually the value of ς_0 are plotted in Figure 2. It can be seen that they meet a very good agreement.

Example 3. Now, nondimensional frequencies of the rotating beam with the speed χ are compared. Consider an cantilever beam with the length L, thickness $h = b = L/100$, $r = 0$, $E = 70$ GPa, and mass density $\rho = 2700$ kg/m^3. The nondimensional frequency is calculated as follows:

$$\widetilde{\omega}_i = \omega_i L^2 \sqrt{\frac{12\rho}{Eh^2}}. \tag{30}$$

Table 1: The comparative frequencies ($\widetilde{\omega}$) of the FGM resting on the two-parameter elastic foundation, $\overline{K}_w = 10$, $\overline{K}_s = 1$, and S-S.

				$a/h = 100$				
				This work				
	n	Mode	Exact [44]	6 elements	8 elements	**10 elements**	12 elements	14 elements
Without elastic foundation $\overline{K}_w = 0$ and $\overline{K}_s = 0$	0	1	5.483	5.483	5.483	**5.483**	5.483	5.483
		2	21.933	21.931	21.924	**21.922**	21.921	21.921
		3	49.350	49.389	49.318	**49.296**	49.288	49.284
	1	1	4.221	4.220	4.220	**4.220**	4.220	4.220
		2	16.884	16.884	16.879	**16.877**	16.876	16.876
		3	37.989	38.030	37.975	**37.958**	37.952	37.949
	2	1	3.852	3.851	3.851	**3.851**	3.851	3.851
		2	15.407	15.408	15.403	**15.402**	15.401	15.401
		3	34.666	34.707	34.657	**34.641**	34.635	34.633
With elastic foundation $\overline{K}_w = 10$ and $\overline{K}_s = 1$	0	1	6.015	6.014	6.014	**6.014**	6.014	6.014
		2	22.445	22.442	22.436	**22.434**	22.433	22.433
		3	49.858	49.891	49.824	**49.803**	49.796	49.792
	1	1	5.008	5.007	5.007	**5.007**	5.007	5.007
		2	17.666	17.664	17.660	**17.659**	17.658	17.658
		3	38.77	38.801	38.753	**38.738**	38.732	38.729
	2	1	4.752	4.752	4.752	**4.752**	4.752	4.752
		2	16.316	16.315	16.311	**16.310**	16.310	16.309
		3	35.577	35.606	35.564	**35.550**	35.545	35.543

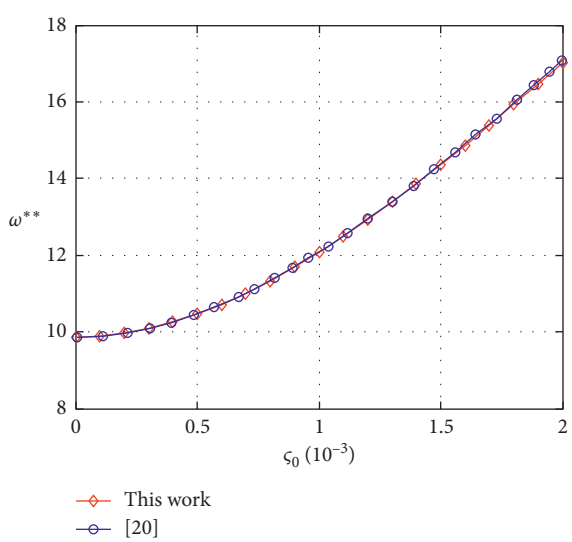

Figure 2: The dependence of first nondimensional frequencies of the S-S FGM beam with initial geometrical imperfection on ς_0.

Table 2 presents the first three nondimensional frequencies of the beam with different rotational speed ratios $\vartheta = L^2\chi\sqrt{12\rho/Eh^2}$ obtained from this work, exact solution [46], new dynamic modeling method (DMM) [47], and isogeometric analysis [15].

Example 4. Finally, this example carries out the comparison of nondimensional frequencies of clamped-clamped FGM (Al_2O_3/SUS304) beams in thermal environments, where $L/h = 20$. Temperature-dependent material properties are presented in Table 3. The nondimensional frequency is calculated as $\breve{\omega}_i = \omega_i L^2\sqrt{\rho_c bh/E_c I}$ (with $I = bh^3/12$). The results of this paper and the exact solutions [48] are shown in Table 4.

4. Numerical Results

This section is about to present the numerical explorations on free vibration analysis of rotating FGM beams in thermal environments, where the initial geometrical imperfection is considered. The beam is resting on a two-parameter elastic foundation. Temperature-dependent material properties are listed in Table 3, and Young's moduli of ceramic and metal changing by temperature are plotted in Figure 3. The imperfection of the beam is $w_0(x) = G_0 \sin(\pi x)$, in which G_0 is the amplitude of the imperfection and the imperfection ratio is $\varsigma_0 = G_0/L$.

The nondimensional frequency of the FGM beam and other parameters are normalized as follows:

Table 2: The first three nondimensional frequencies ($\tilde{\omega}_i$) of the C-F beam with different rotational speed ratios ϑ.

Mode	Method	Rotation speed ratio ϑ			
		$\vartheta = 0$	$\vartheta = 3$	$\vartheta = 6$	$\vartheta = 12$
$\tilde{\omega}_1$	This work	3.5161	4.6790	7.0734	12.6098
	Exact [46]	3.5160	4.7973	7.3604	13.1702
	DMM [47]	3.5160	4.7973	7.3604	—
	Isogeometric [15]	3.5118	4.7733	7.3276	—
$\tilde{\omega}_2$	This work	22.0247	23.1197	26.1110	36.4500
	Exact [46]	22.0345	23.3203	26.8091	37.6031
	DMM [47]	—	—	—	—
	Isogeometric [15]	—	—	—	—
$\tilde{\omega}_3$	This work	61.6254	62.7602	66.0242	77.4512
	Exact [46]	61.6972	62.9850	66.6840	79.6145
	DMM [47]	—	—	—	—
	Isogeometric [15]	—	—	—	—
$\tilde{\omega}_4$	This work	120.647	121.843	125.348	138.295
	Exact [46]	120.902	122.236	126.140	140.534
	DMM [47]	—	—	—	—
	Isogeometric [15]	—	—	—	—

Table 3: Temperature-dependent material properties [40].

Materials	P_0	P_{-1}	P_1	P_2	P_3	P (300 K)
Ceramic aluminum oxide (Al_2O_3)						
E (Pa)	349.55e9	0	_3.853e_4	4.027e_7	_1.673e_10	320.24e9
α (1/K)	6.8269e_6	0	1.838e_4	0	0	7.203e_6
ν	0.26	0	0	0	0	0.260
ρ (kg/m^3)	3800	0	0	0	0	3800
Metal stainless steel SUS304						
E (Pa)	201.04e9	0	3.079e_4	_6.534e_7	0	207.79e9
α (1/K)	12.330e_6	0	8.086e_4	0	0	15.321e_6
ν	0.326	0	_2.002e_4	3.797e_7	0	0.318
ρ (kg/m^3)	8166	0	0	0	0	8166

$$\omega_i^* = \omega_i L^2 \sqrt{\frac{12\rho_0}{E_0 h^2}},$$

$$K_w^* = \frac{k_w L^4}{D_0},$$

$$K_s^* = \frac{k_s L^2}{D_0},$$

$$\eta = L^2 \chi \sqrt{\frac{12\rho_0}{E_0 h^2}},$$

$$D_0 = \frac{E_0 h^3}{12}, \quad \text{with } \rho_0 = 3800\text{kg/m}^3, E_0 = 3.2024.10^{11}\ \text{N/m}^2. \tag{31}$$

4.1. Free Vibration Explorations

4.1.1. Effect of Rotational Speed. Consider a geometrically imperfect beam with dimensions $L/h = 20$, imperfect parameter $\varsigma_0 = 0.001$, $K_w^* = 10$, $K_s^* = 1$, distance ratio $r/L = 0$, and $\Delta T = 20$ K. Changing the value of the rotational speed χ of the beam so that η varies in a range of 0 to 10, and the volume fraction index n gets the values from 0 to 10. The dependences of the first three frequencies of C-F and S-S beams on the rotational speed and volume fraction index are presented in Figures 4 and 5. Figure 6 shows the dependence of the first frequency of the FGM beam on the distance ratio r/L and the rotational speed. Figures 7 and 8 present the first frequency of the S-S beam on the distance ratio r/L and the rotational speed, and the first four frequencies of S-S and C-F beams depending on the rotational speed are presented in Figure 9. Based on these numerical results, some conclusions are drawn as follows:

(i) Frequencies of the FGM beam increase when the value of the rotational speed increases. This can be explained that when the beam is rotating, the centrifugal force will appear; therefore, the stiffness of the structure will increase. Besides, when increasing the volume fraction index n, the proportion of metal increases, the beam becomes softer, so the frequency of the beam is reduced.

(ii) With the increasing of the distance ratio r/L, the frequency of the beam is also enhanced, and this phenomenon presents more clearly when the rotational speed gets higher value. Figure 5 shows that

Table 4: The dependence of nondimensional frequencies $\breve{\omega}_i$ of clamped-clamped FGM beams in the thermal environment on the volume fraction index n, L/h = 20.

$\Delta T\,(K)$	$\breve{\omega}_i$	n							
		0		0.2		1		5	
		Exact [48]	This work	Exact [48]	This work	Exact [48]	This work	Exact [23]	This work
0	1	22.3447	22.0003	19.6819	19.3997	16.0094	15.8072	13.7110	13.5306
	2	61.3790	59.6498	54.0567	52.6094	43.9727	42.8791	37.6706	36.6636
20	1	22.1532	21.8079	19.4789	19.1986	15.7954	15.5992	13.4954	13.3222
	2	61.1205	59.3870	53.7827	52.3393	43.6841	42.6058	37.3801	36.3926
40	1	21.9585	21.6122	19.2695	18.9915	15.5703	15.3809	13.2663	13.1010
	2	60.8590	59.1212	53.4998	52.0612	43.3779	42.3176	37.0678	36.1027

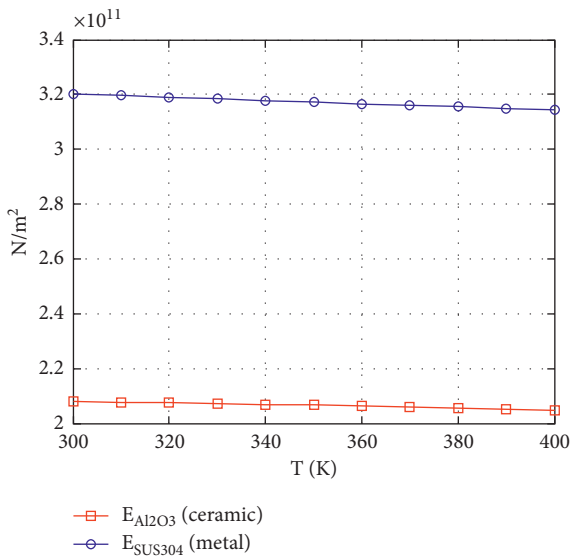

Figure 3: The dependence of Young's moduli of ceramic (Al_2O_3) and metal (SUS304) on temperature.

when the beam rotates at a small speed, the difference of the first natural frequency with different values of distance r is not much; the greater the speed, the more this difference is.

(iii) Both rotational speed and distance r affect the vibration mode shapes of the FGM beam, especially to the first frequency. From Figure 6, the readers can find that, as the distance r increases, the first vibration mode shape of the beam tends to deviate to the right due to the influence of the greater inertial force. This shows that the distance r and the rotational speed of the beam have a significant effect on the frequency as well as the vibration mode shape of the structure.

4.1.2. Influence of the Temperature. In this section, the influence of the temperature on the free vibration response of the beam is evaluated. Consider a geometrically imperfect beam with geometrical parameters $L/h = 20$, imperfect parameter $\varsigma_0 = 0.001$, $K_w^* = 10$, $K_s^* = 1$, distance ratio $r/L = 0$, and rotational speed $\eta = 5$ changing the temperature so that $\Delta T = 0 - 100$ K, and the volume fraction index $n = 0$–10. The dependence of the first three dimensional frequencies of the cantilever FGM beam on the temperature and volume fraction index n is shown in Figure 10. The first three dimensional frequencies of C-F and S-S FGM beams on the temperature and rotational speed are presented in Figure 11. Some discussions of these numerical results are drawn as follows:

(i) When increasing the temperature, frequencies of FGM beams decrease. This can be explained that Young's moduli of ceramic and metal decrease as the temperature increases; therefore, the structure becomes softer.

(ii) When the value of the rotational speed is small, the effect of the centrifugal force presents slightly; thus, the slope of the dependence curve of frequency on the temperature is higher. Besides, the higher the speed of the beam is, the more clearly is the frequency dependence on the temperature shown is.

4.1.3. Influence of the Imperfect Ratio. Next, the influence of the imperfect ratio is investigated. Consider a geometrically imperfect beam with $L/h = 20$, $K_w^* = 10$, $K_s^* = 1$, distance ratio $r/L = 2$, rotational speed $\eta = 10$, temperature $\Delta T = 20$ K, the initial imperfect parameter ς_0 changes in a range of 0 to 0.002, and the volume fraction index $n = 0$–10. Figure 12 plotted the first three vibration mode shapes of FGM beams on the initial imperfect parameter and volume fraction index. Figure 13 presents the dependence of the first three frequencies on the initial imperfect parameter, temperature, and rotational speed. One can see as follows:

(i) When increasing the initial imperfect parameter ς_0 of the beam, frequencies increase; however, this change is presented very slightly

(ii) For each value of the initial imperfect parameter ς_0, the change of the frequency of the FGM beam is presented most when the volume fraction n gets the values in a range of 0 to 2

4.1.4. Influence of Elastic Foundation Parameters. This last investigation is about to evaluate the effect of elastic foundation parameters on vibration responses of FGM beams. To see more of this influence, the two following parameters are changed as follows: K_w^* varies in a range of 0 to 20 and K_s^* gets the values from 0 to 2. The first

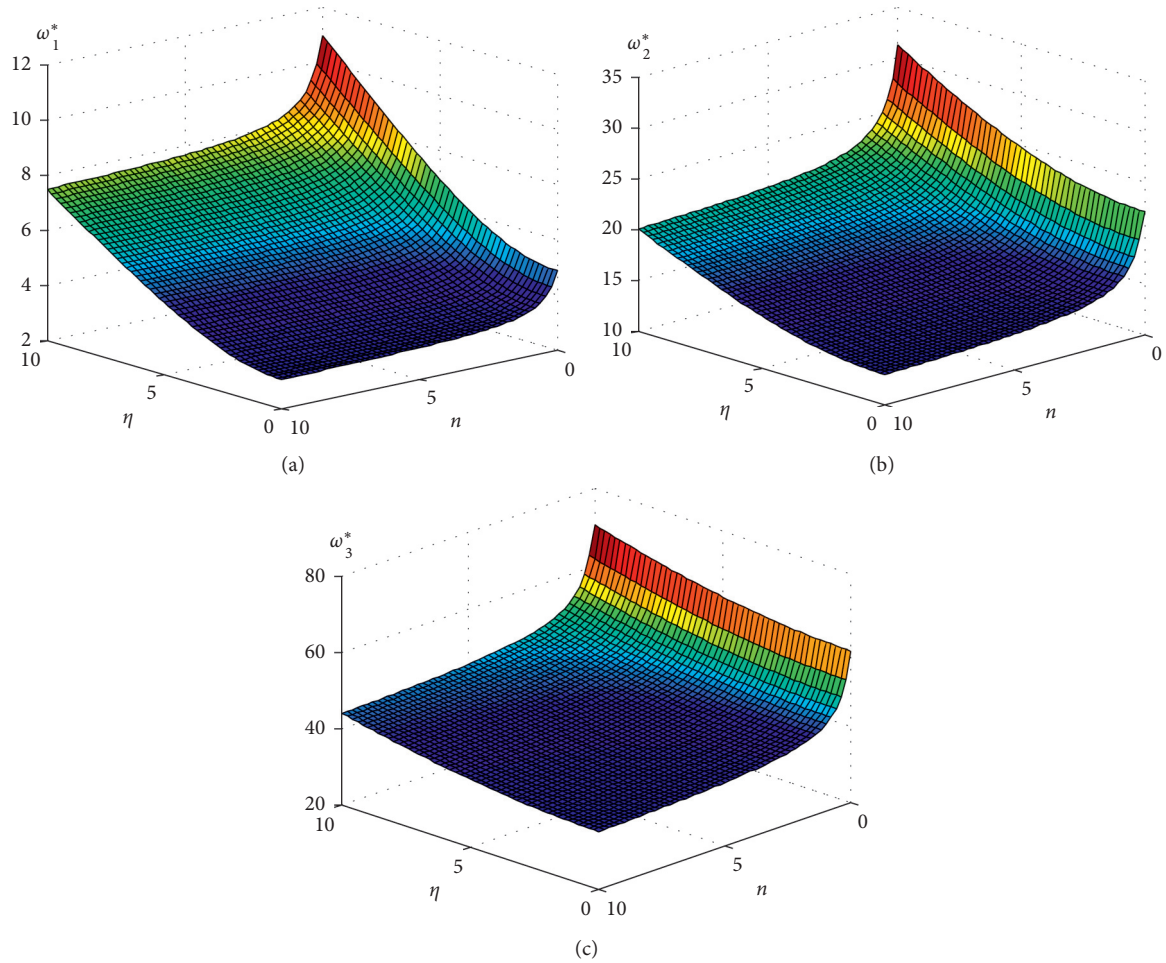

Figure 4: The dependence of the first three nondimensional frequencies of the C-F geometrically imperfect beam (C-F) on the rotational speed and n, $\varsigma_0 = 0.001$, $K_w^* = 10$, and $K_s^* = 1$. (a) The first frequency. (b) The second frequency. (c) The third frequency.

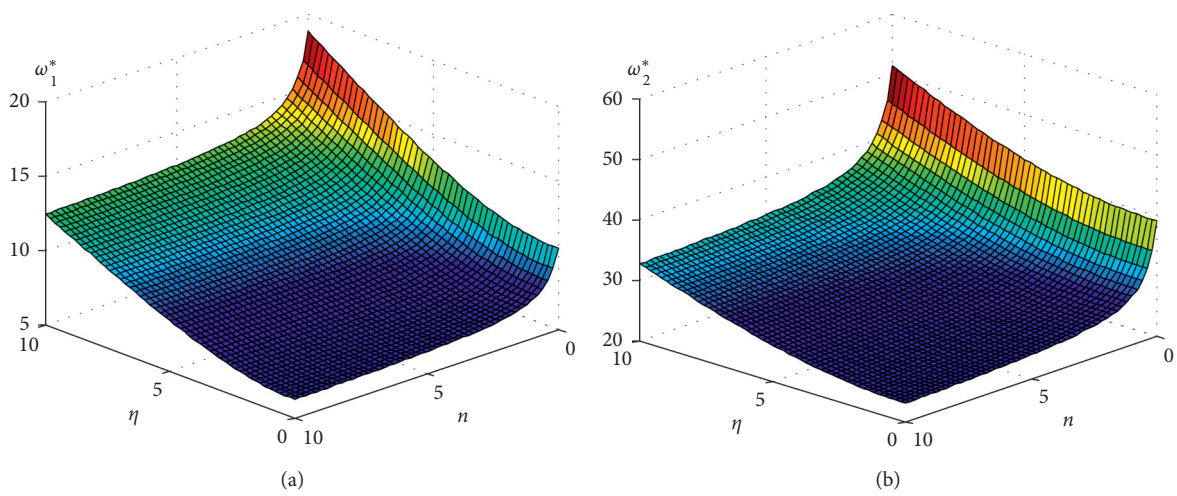

Figure 5: Continued.

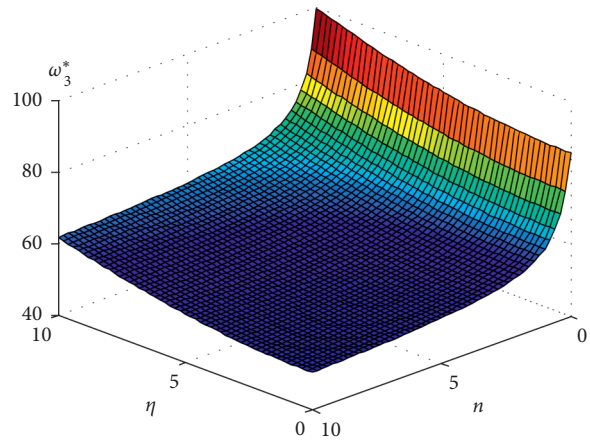

(c)

Figure 5: The dependence of the first three nondimensional frequencies of the C-F geometrically imperfect beam (S-S) on the rotational speed and n, $\varsigma_0 = 0.001$, $K_w^* = 10$, and $K_s^* = 1$. (a) The first frequency. (b) The second frequency. (c) The third frequency.

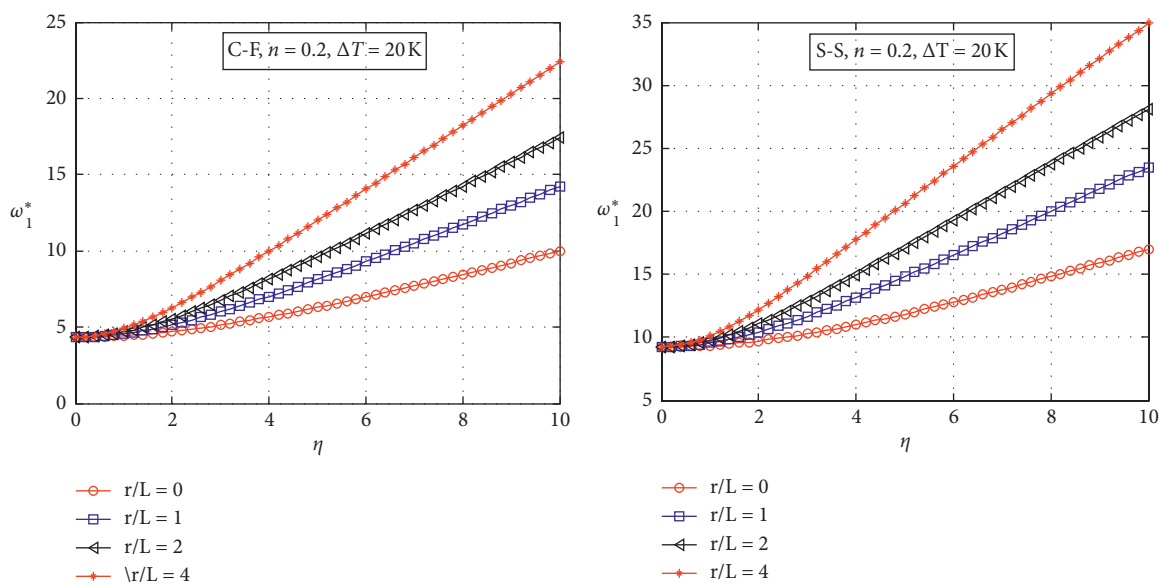

(a) (b)

Figure 6: The dependence of the first nondimensional frequency of the geometrically imperfect FGM beam on the distance ratio r/L.

nondimensional frequencies of FGM beams are listed in Tables 5 and 6, where these parameters are taken into calculations: $L/h = 20$, distance ratio $r/L = 2$, rotational speed $\eta = 10$, temperature $\Delta T = 20$ K, and initial imperfect parameter $\varsigma_0 = 0.001$. It can be observed that when increasing the elastic foundation parameters, the stiffness of the structure increases; as a result, nondimensional frequencies of FGM beams increase correspondingly. Similarly, one can see that when the volume fraction index n changes in a range of 0 to 2, the change of nondimensional frequencies is presented more sharply. This changed is faded gradually when n gets the values from 2 to 10.

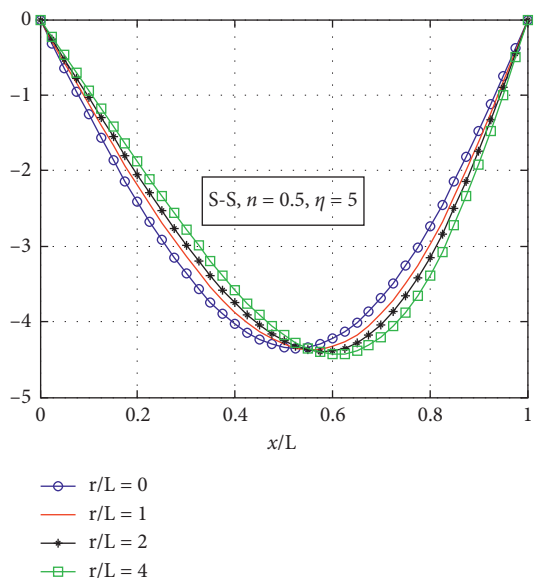

Figure 7: The dependence of the first vibration mode shape of the geometrically imperfect FGM beam on the distance ratio r/L.

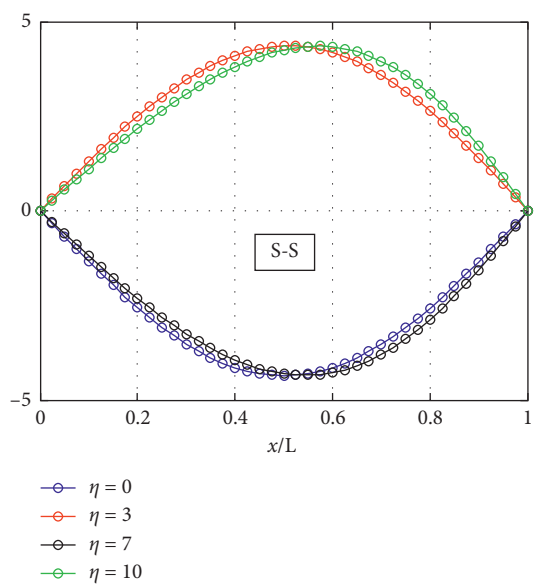

Figure 8: The first vibration mode shape of the FGM beam depends on the rotational speed, $n = 0.5$ and $r = 0$.

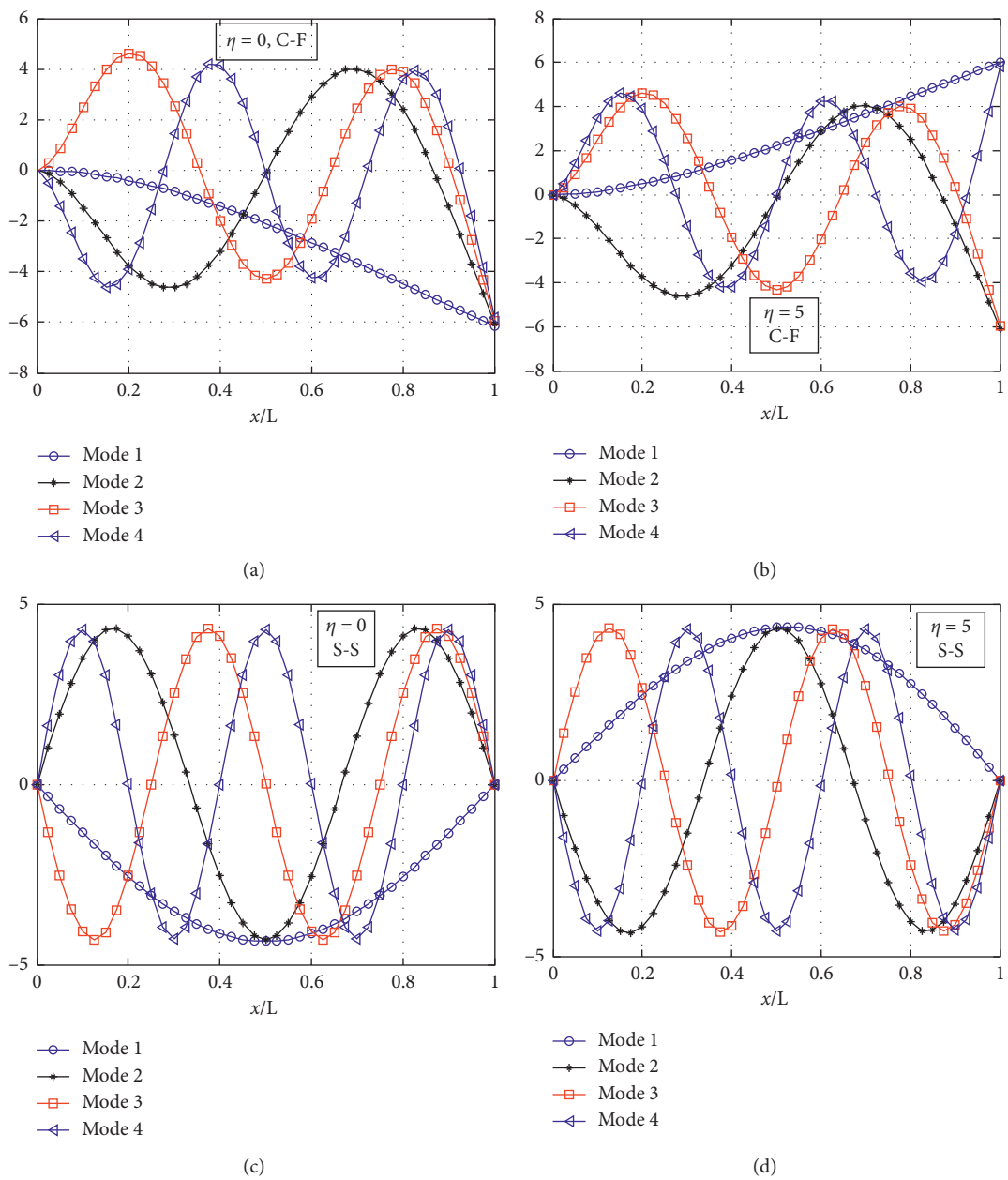

Figure 9: The dependence of the first four vibration mode shapes of the FGM beam on the rotational speed, $n = 0.5$ and $r = 0$. (a) C-F, $\eta = 0$, and $r = 0$. (b) C-F, $\eta = 5$, and (r) = 0. (c) S-S, $\eta = 0$, and $r = 0$. (d) S-S, $\eta = 5$, and $r = 0$.

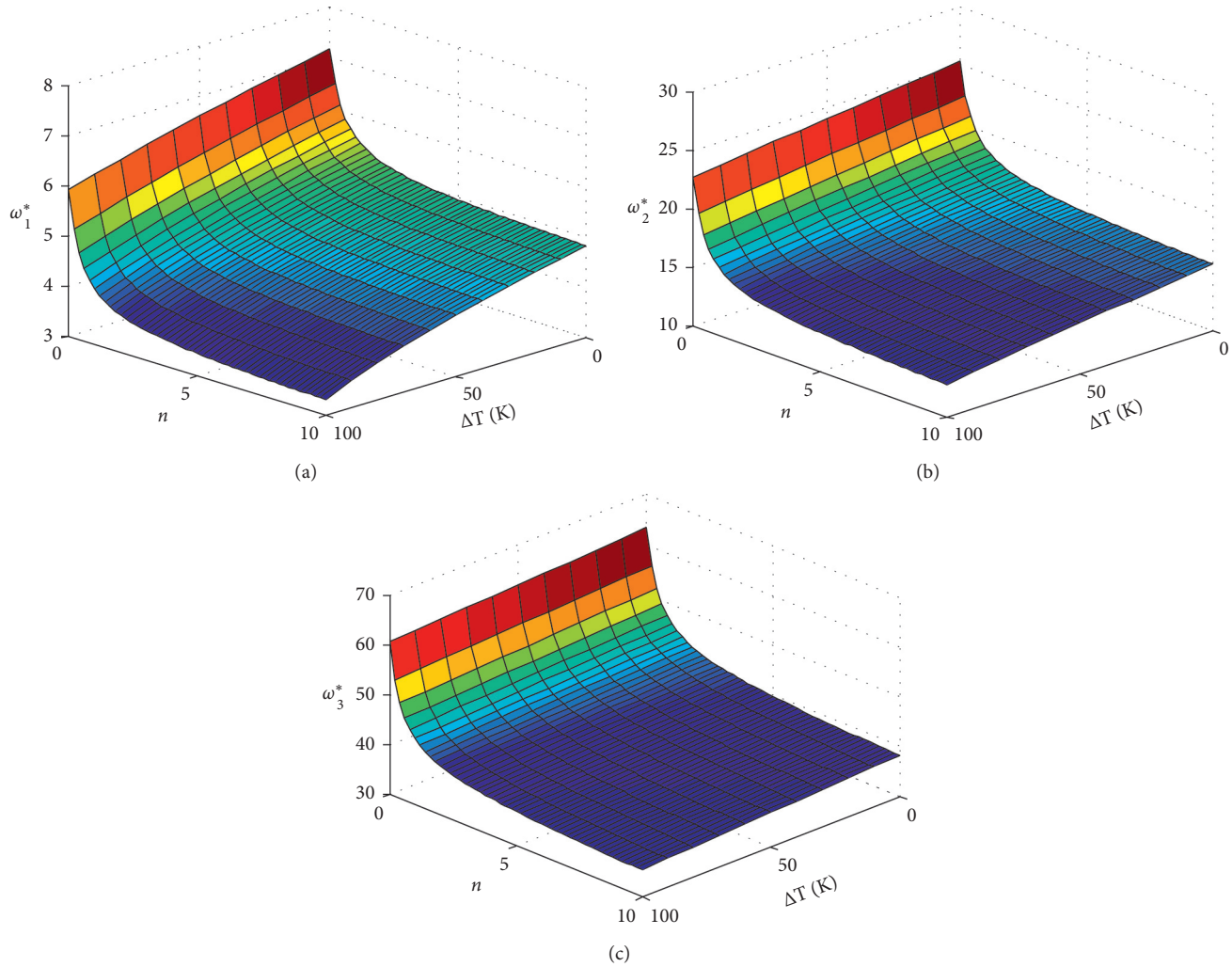

Figure 10: The dependence of the first three frequencies of the cantilever FGM beam on the temperature, $r/L = 0$ and $\eta = 5$. (a)ω_1^*. (b)ω_2^*. (c)ω_3^*.

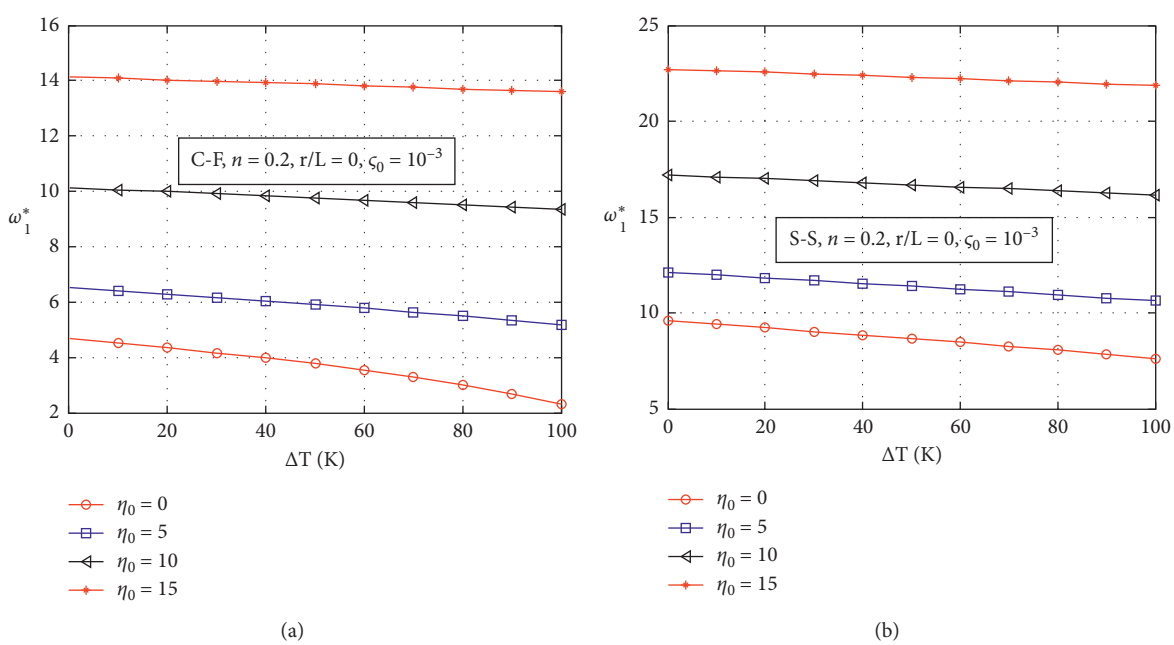

Figure 11: The dependence of the first frequency of FGM beams on the temperature and rotational speed. (a) C-F. (b) S-S.

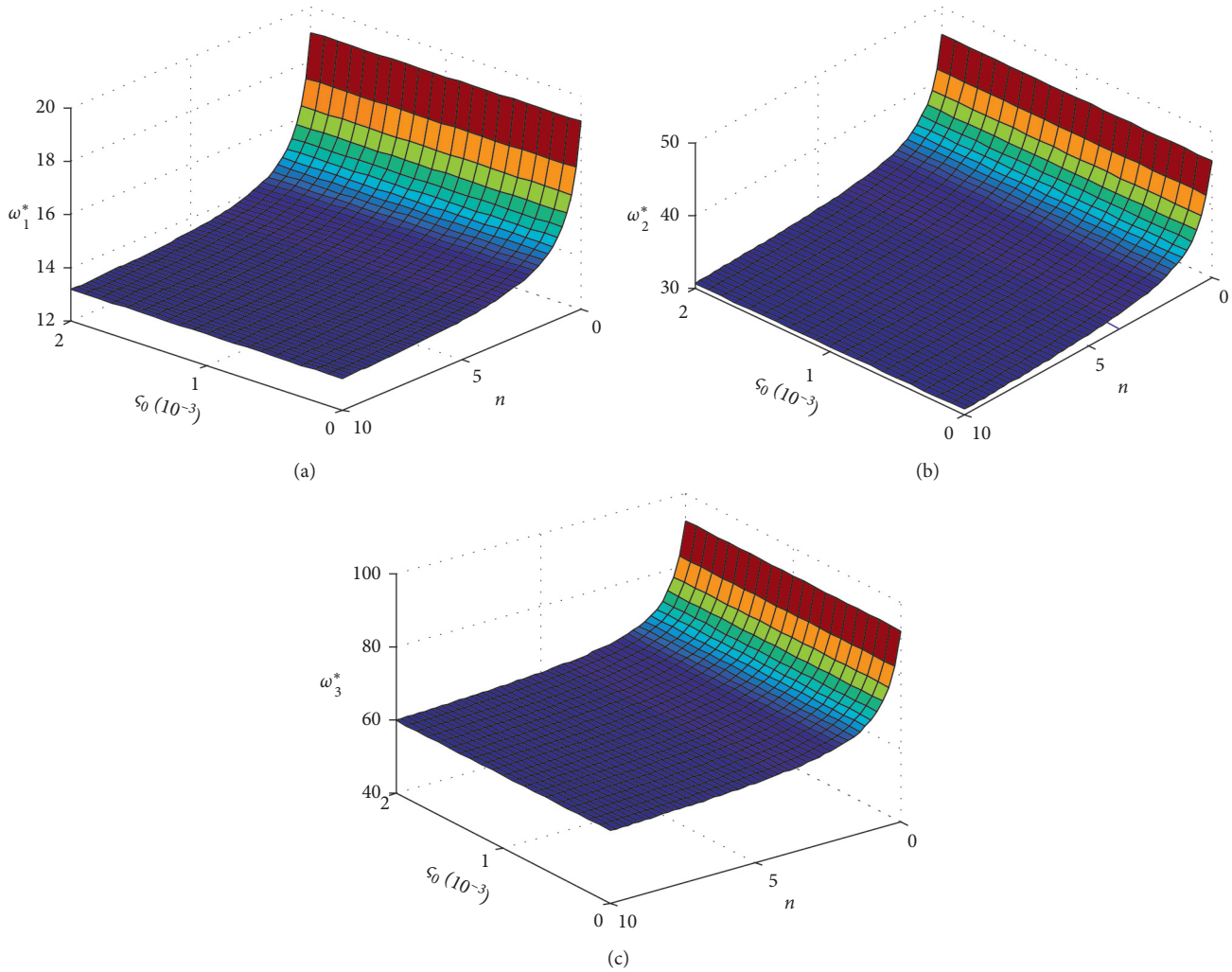

Figure 12: The first three nondimensional frequencies of the cantilever FGM beam on the initial imperfect parameter ς_0. (a)ω_1^*. (b)ω_2^*. (c)ω_3^*.

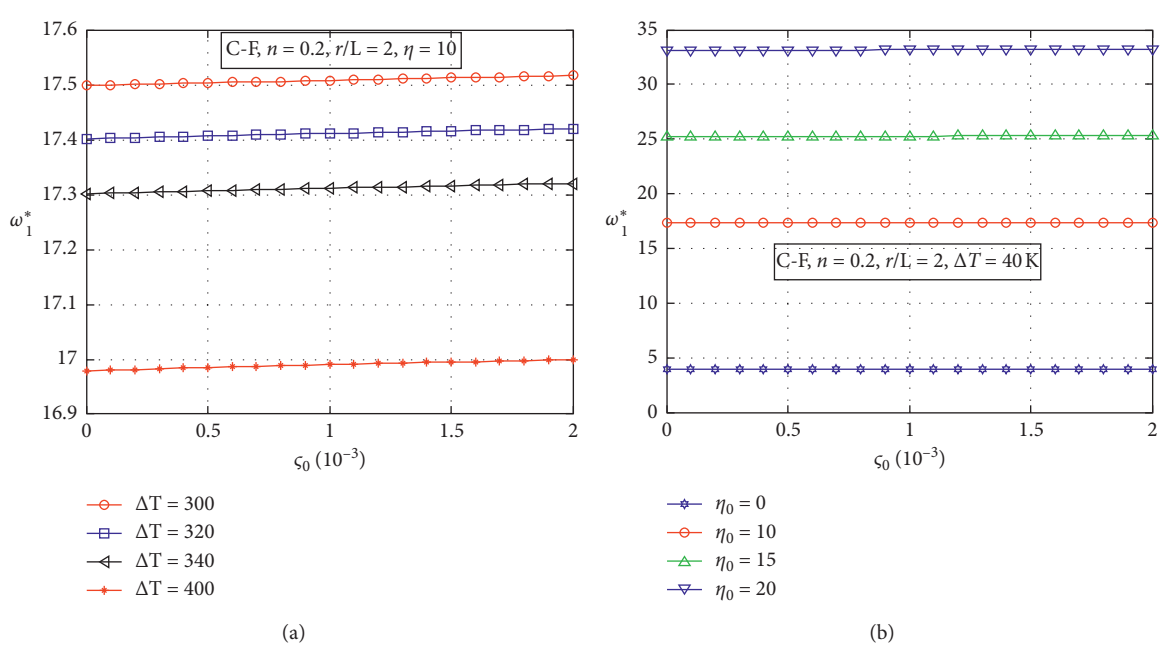

Figure 13: The first nondimensional frequency of the cantilever FGM beam on the initial imperfect parameter ς_0 and the temperature.

Table 5: The first nondimensional frequency of the cantilever FGM beam depends on K_w^* and K_s^*.

K_w^*	K_s^*	n					
		0	0.2	1	2	5	10
0	0	18.6497	17.0410	14.7543	13.9080	13.1900	12.8903
	1	18.7891	17.1703	14.8700	14.0184	13.2956	12.9943
	2	18.9239	17.2951	14.9814	14.1244	13.3970	13.0941
10	0	18.9155	17.2852	14.9677	14.1099	13.3821	13.0784
	1	19.0530	17.4127	15.0818	14.2187	13.4862	13.1810
	2	19.1860	17.5358	15.1916	14.3233	13.5861	13.2793
20	0	19.1777	17.5259	15.1781	14.3089	13.5714	13.2639
	1	19.3133	17.6517	15.2907	14.4162	13.6741	13.3650
	2	19.4445	17.7732	15.3990	14.5194	13.7726	13.4620

Table 6: The first nondimensional frequency of the S-S FGM beam depends on K_w^* and K_s^*.

K_w^*	K_s^*	n					
		0	0.2	1	2	5	10
0	0	30.5631	27.7426	23.7399	22.2960	21.0839	20.5570
	1	30.7569	27.9238	23.9039	22.4529	21.2347	20.7058
	2	30.9489	28.1035	24.0662	22.6082	21.3838	20.8530
10	0	30.7259	27.8930	23.8730	22.4223	21.2044	20.6753
	1	30.9186	28.0733	24.0360	22.5784	21.3543	20.8233
	2	31.1097	28.2520	24.1975	22.7328	21.5026	20.9697
20	0	30.8878	28.0427	24.0053	22.5479	21.3243	20.7930
	1	31.0795	28.2220	24.1674	22.7031	21.4733	20.9401
	2	31.2696	28.3998	24.3280	22.8567	21.6208	21.0857

5. Conclusions

This paper uses a combination of the simple shear deformation theory (type hyperbolic sine functions) and the finite element method to establish the finite element formulations of the free vibration problem of rotating FGM beams resting on two-parameters' elastic foundations, in which the effects of the initial geometrical imperfection and temperature are taken into calculations. The numerical results of this work are truly novel explorations, which can be used in computational design and in practical engineering.

(i) When the speed of rotation of the FGM beam increases, the inertial force increases; therefore, the frequencies of the structure increase. The rotational speed has a significant influence on the vibration responses of the beam. In addition, the distance r from the top of the beam to the axis of rotation also has a significant influence on the natural frequency of the beam; the greater the distance, the greater the frequency of the beam. At the same time, the shape of the first natural frequency tends to move to the right as this distance increases.

(ii) As the temperature increases, the mechanical properties of the material change and the elastic modulus decreases; as a result, the frequencies of the FGM beam also decrease.

(iii) The nondimensional frequencies of FGM beams increase when the initial imperfect parameter increases slightly. Also, as the elastic foundation parameters increase, nondimensional frequencies of FGM beams enhance. The change of nondimensional frequencies is presented most when the volume fraction index n gets the values in a range of 0 to 2.

From the numerical results of this study, the design and use of a rotating beam structure performing in a temperature environment need to pay attention to many parameters, in which special attention should be paid to the rotation speed of the beam and the distance r from the top of the beam to the fixed axis.

Data Availability

Data used to support the findings of this study are included within the article.

Conflicts of Interest

All authors declare that there are no conflicts of interest regarding the publication of this paper.

Acknowledgments

This work was supported by the University of Transport Technology Foundation for Science and Technology Development (Grant no. 1139/QD-DHCNGTVT).

References

[1] J. N. Reddy, "Free vibration analysis of functionally graded ceramic-metal plates," *Analysis and Design of Plated Structures*, vol. 1, pp. 293–321, 2007.

[2] Z. Ning, K. Tahir, G. Haomin, S. Shaoshuai, Z. Wei, and Z. Weiwei, "Functionally graded materials: an overview of stability, buckling, and free vibration analysis," *Advances in Materials Science and Engineering*, vol. 2019, Article ID 1354150, 18 pages, 2019.

[3] D. V. Thom, D. H. Duc, P. V. Minh, and N. S. Tung, "Finite element modelling for free vibration response of cracked stiffened FGM plates," *Vietnam Journal of Science and Technology*, vol. 58, no. 1, pp. 119–129, 2020.

[4] V. T. Do, D. K. Nguyen, N. D. Duc, D. H. Doan, and Q. T. Bui, "Analysis of bi-directional functionally graded plates by FEM and a new third-order shear deformation plate theory," *Thin-Walled Structures*, vol. 119, pp. 687–699, 2017.

[5] H.-N. Nguyen, T. C. Tan, D. T. Luat, V.-D. Phan, D. V. Thom, and P. V. Minh, "Research on the buckling behavior of functionally graded plates with stiffeners based on the third-order shear deformation theory," *Materials*, vol. 12, no. 8, p. 1262, 2019.

[6] S. K. Gunjal and U. S. Dixit, "Vibration analysis of shape-optimized rotating cantilever beams," *Engineering Optimization*, vol. 39, no. 1, pp. 105–123, 2007.

[7] S. C. Pradhan and T. Murmu, "Application of nonlocal elasticity and DQM in the flapwise bending vibration of a rotating nanocantilever," *Physica E: Low-Dimensional Systems and Nanostructures*, vol. 42, no. 7, pp. 1944–1949, 2010.

[8] L. Li, D. G. Zhang, and W. D. Zhu, "Free vibration analysis of a rotating hub–functionally graded material beam system with the dynamic stiffening effect," *Journal of Sound and Vibration*, vol. 333, no. 5, pp. 1526–1541, 2014.

[9] M. D. S. Amir, B. J. Mehdi, and M. Dehrouyeh, "On size-dependent lead-lag vibration of rotating microcantilevers," *International Journal of Engineering Science*, vol. 101, pp. 50–63, 2016.

[10] L. Jung-Woo and L Jung-Youn, "In-plane bending vibration analysis of a rotating beam with multiple edge cracks by using the transfer matrix method," *Meccanica*, vol. 52, pp. 1143–1157, 2017.

[11] D. Das, "Free vibration and buckling analyses of geometrically non-linear and shear-deformable FGM beam fixed to the inside of a rotating rim," *Composite Structures*, vol. 179, pp. 628–645, 2017.

[12] X. Xu, Q. Han, F. Chu, and R. G. Parker, "Vibration suppression of a rotating cantilever beam under magnetic excitations by applying the magnetostrictive material," *Journal of Intelligent Material Systems and Structures*, vol. 30, no. 4, pp. 576–592, 2019.

[13] B. Alireza and X. Y. Cai, "Vibration analysis of rotating rods based on the nonlocal elasticity theory and coupled displacement field," *Microsystem Technologies*, vol. 25, pp. 1077–1085, 2019.

[14] L. Li, W.-H. Liao, D. Zhang, and Y. Zhang, "Vibration control and analysis of a rotating flexible FGM beam with a lumped mass in temperature field," *Composite Structures*, vol. 208, pp. 244–260, 2019.

[15] C. Dejin, F. Kai, and Z. Shijie, "Flapwise vibration analysis of rotating composite laminated timoshenko microbeams with geometric imperfection based on a re-modified couple stress theory and isogeometric analysis," *European Journal of Mechanics-A/Solids*, vol. 76, pp. 25–35, 2019.

[16] M. S. Atanasov and V. Stojanović, "Nonlocal forced vibrations of rotating cantilever nano-beams," *European Journal of Mechanics-A/Solids*, vol. 79, Article ID 103850, 2020.

[17] M. H. Jalaei and Ö. Civalek, "On dynamic instability of magnetically embedded viscoelastic porous FG nanobeam," *International Journal of Engineering Science*, vol. 143, pp. 14–32, 2019.

[18] Ç. Demir and Ö. Civalek, "On the analysis of microbeams," *International Journal of Engineering Science*, vol. 121, pp. 14–33, 2017.

[19] B. Akgöz and Ö. Civalek, "A novel microstructure-dependent shear deformable beam model," *International Journal of Mechanical Sciences*, vol. 99, pp. 10–20, 2015.

[20] L. Hanten, G. Giunta, S. Belouettar, and V. Salnikov, "Free vibration analysis of fibre-metal laminated beams via hierarchical one-dimensional models," *Mathematical Problems in Engineering*, vol. 2018, Article ID 2724781, 12 pages, 2018.

[21] G. Moustafa, S. Hayat, B. Fouad et al., "Influences of porosity distributions and boundary conditions on mechanical bending response of functionally graded plates resting on Pasternak foundation," *Steel and Composite Structures*, vol. 38, no. 1, pp. 1–15, 2021.

[22] R. Abdelkrim, C. Abdelbaki, A. B. Abdelmoumen et al., "Physical stability response of a SLGS resting on viscoelastic medium using nonlocal integral first-order theory," *Steel and Composite Structures*, vol. 37, no. 6, pp. 695–709, 2020.

[23] B. Noureddine, Z. Mohamed, A. B. Abdelmoumen et al., "Deflections, stresses and free vibration studies of FG-CNT reinforced sandwich plates resting on Pasternak elastic foundation," *Computers and Concrete*, vol. 26, no. 3, pp. 213–226, 2020.

[24] R. Mohamed, H. B. Kouider, K. Abdelhakim et al., "A new innovative 3-unknowns HSDT for buckling and free vibration of exponentially graded sandwich plates resting on elastic foundations under various boundary conditions," *Geomechanics and Engineering*, vol. 22, no. 2, pp. 119–132, 2020.

[25] B. Fouad, A. B. Abdelmoumen, T. Abdeldjebbar et al., "Stability and dynamic analyses of SW-CNT reinforced concrete beam resting on elastic-foundation," *Computers and Concrete*, vol. 25, no. 6, pp. 485–495, 2020.

[26] C. C. Sara, K. Abdelhakim, A. B. Abdelmoumen et al., "A novel four-unknown integral model for buckling response of FG sandwich plates resting on elastic foundations under various boundary conditions using Galerkin\'s approach," *Geomechanics and Engineering*, vol. 21, no. 5, pp. 471–487, 2020.

[27] R. Salah, A. B. Abdelmoumen, B. Abdelhakim et al., "Effects of hygro-thermo-mechanical conditions on the buckling of FG sandwich plates resting on elastic foundations," *Computers and Concrete*, vol. 25, no. 4, pp. 311–325, 2020.

[28] K. Miloud, K. Abdelhakim, A. B. Abdelmoumen et al., "A study on the structural behaviour of functionally graded porous plates on elastic foundation using a new quasi-3D model: bending and free vibration analysis," *Computers and Concrete*, vol. 25, no. 1, pp. 37–57, 2020.

[29] T. Abdelouahed, S. U. Al-Dulaijan, M. A. Al-Osta et al., "A four variable trigonometric integral plate theory for hygro-thermo-mechanical bending analysis of AFG ceramic-metal plates resting on a two-parameter elastic foundation," *Steel and Composite Structures*, vol. 34, no. 4, pp. 511–524, 2020.

[30] Y. A. Farouk, M. Mustapha, A. B. Abdelmoumen et al., "Influences of porosity on dynamic response of FG plates resting on Winkler/Pasternak/Kerr foundation using quasi

3D HSDT," *Computers and Concrete*, vol. 24, no. 4, pp. 347–367, 2019.

[31] B. Hichem, M. S. Mahmoud, C. Abdelbaki et al., "Influence of porosity on thermal buckling behavior of functionally graded beams," *Smart Structures and Systems*, vol. 27, no. 4, pp. 719–728, 2021.

[32] A. Ehsan, K. Mohammad, Z. Soleimani-Javid, A. Saeed, and T. Abdelouahed, "Porosity-dependent vibration analysis of FG microplates embedded by polymeric nanocomposite patches considering hygrothermal effect via an innovative plate theory," *Engineering With Computers*, 2021.

[33] M. S. H. Al-Furjan, H. Mostafa, R. Alireza et al., "Chaotic simulation of the multi-phase reinforced thermo-elastic disk using GDQM," *Engineering With Computers*, 2020.

[34] M. Hakima, A. B. Abdelmoumen, H. Houari et al., "Investigation on hygro-thermal vibration of P-FG and symmetric S-FG nanobeam using integral Timoshenko beam theory," *Advances in Nano Research*, vol. 8, no. 4, pp. 293–305, 2020.

[35] B. Abderrafik, B. Belhadj, B. Mohamed et al., "A simple nth-order shear deformation theory for thermomechanical bending analysis of different configurations of FG sandwich plates," *Smart Structures and Systems*, vol. 25, no. 2, pp. 197–218, 2020.

[36] T. Yu, T. Q. Bui, S. Yin et al., "On the thermal buckling analysis of functionally graded plates with internal defects using extended isogeometric analysis," *Composite Structures*, vol. 136, pp. 684–695, 2016.

[37] P. T. Dat, D. V. Thom, and D. T. Luat, "Free vibration of functionally graded sandwich plates with stiffeners based on the third-order shear deformation theory," *Vietnam Journal of Mechanics*, vol. 38, no. 2, pp. 103–122, 2016.

[38] N. D. Duc, T. D. Trinh, T. Van Do, and D. H. Doan, "On the buckling behavior of multi-cracked FGM plates," in *Proceedings of the International Conference on Advances in Computational Mechanics 2017*, pp. 29–45, Phu Quoc Island, Vietnam, August 2018.

[39] V. T. Do, D. H. Doan, N. D. Duc, and T. Q. Bui, "Phase-field thermal buckling analysis for cracked functionally graded composite plates considering neutral surface," *Composite Structures*, vol. 182, pp. 542–548, 2017.

[40] Q. B. Tinh, V. D. Thom, H. T. T. Lan et al., "On the high temperature mechanical behaviors analysis of heated functionally graded plates using FEM and a new third-order shear deformation plate theory," *Composites Part B: Engineering*, vol. 92, pp. 218–241, 2016.

[41] K. P. Soldatos, "A transverse shear deformation theory for homogeneous monoclinic plates," *Acta Mechanica*, vol. 94, no. 3-4, pp. 195–220, 1992.

[42] T. Huu-Tai and C. Dong-Ho, "Finite element formulation of various four unknown shear deformation theories for functionally graded plates," *Finite Elements in Analysis and Design*, vol. 75, pp. 50–61, 2013.

[43] S. P. Timoshenko and J. M. Gere, *Theory of Elastic Stability*, Dover Publications, Mineola, NY, USA, 1989.

[44] M. Avcar and K. M. M. Waleed, "Free vibration of functionally graded beams resting on Winkler-Pasternak foundation," *Arabian Journal of Geosciences*, vol. 11, no. 232, 2018.

[45] M. H. Ghayesh and M. Amabili, "Coupled longitudinal-transverse behaviour of a geometrically imperfect microbeam," *Composites Part B: Engineering*, vol. 60, pp. 371–377, 2014.

[46] A. D. Wright, C. E. Smith, R. W. Thresher, and J. L. C. Wang, "Vibration modes of centrifugaily stiffened beams," *Journal of Applied Mechanics*, vol. 49, no. 1, pp. 197–202, 1982.

[47] H. H. Yoo and S. H. Shin, "Vibration analysis of rotating cantilever beams," *Journal of Sound and Vibration*, vol. 212, no. 5, pp. 807–828, 1998.

[48] F. Ebrahimi and E. Salari, "Thermo-mechanical vibration analysis of nonlocal temperature-dependent FG nanobeams with various boundary conditions," *Composites Part B: Engineering*, vol. 78, pp. 272–290, 2015.